◉論 文

Numerical Modeling of Short-Time Scale Nonlinear Water Waves Generated by Large Vertical Motions of Non-Wallsided Bodies

Jong-Hwan Park* · Armin W. Troesch**

(1992년 10월 26일 접수)

Non-Wallsided 물체의 연직운동에 의해 발생된 파의 비선형 해석을 위한 수치해석 모형의 연구

박 종 환* · 아민 트로쉬**

Key Words : Boundary Integral Method(BIM), CFL number, Free Surface Stability number, Impact force, Matrix Stability Analysis, Mixed Eulerian-Lagrangian Method, Nonlinear Ship Motion, Numerical Stability, Saw-tooth Instability, von-Neumann Analysis, Wedge-shaped body.

Abstract

선수충격파의 문제를 푸는데 있어서 Boundary Integral Method(BIM)의 여러가지 수치해석방법이 검토되었으며, 특히 여러가지 Time Stepping Scheme, Green function, far-field 조건등에 따른 수치해석안정성과 정확성의 상관관계가 연구되었다.

von Neumann 안정성해석과 matrix 안정성해석 등을 이용한 선형 안정성해석을 기초로 하여, 수치해석방법의 안정성 여부를 체계적으로 조사할 수 있는 parameter(Free Surface Stability number)를 설정하고, 이 parameter의 변화에 따른 비선형 운동해석을 연구하였다. 그 결과 비선형성이 심하지 않은 기진파의 경우에서는 비선형 운동해석의 수치해석 안정성이 선형 수치해석 안정성과 큰 차이가 없음을 알 수 있게 된다.

NOMENCLATURE

β	Phase($k\Delta x$)
Δx	Panel length
Δt	Time interval between time step
ϕ_i^n	Velocity potential of ith location at the nth time step

* Post Doc in KRISO

** Associate Professor of Department of Naval Architecture and Marine Engineeing, University of Michigan, Ann Arbor, Michigan 48109.

$\vec{\xi}$	Source point vector(ξ, η, ζ)
η^n_i	Free surface elevation of the ith location at the nth time step
[A], [B]	Induced influence coefficient matrices
c	Green function constant, e.g. $G^*_{2D} = G_{2D} + \ln c$
{f}	Equivalent excitation vector
FSS	Free Surface Stability Number $(\frac{(\pi g \Delta t)^2}{\Delta x})$
$G(\vec{x} ; \vec{\xi})$	Green function
G	Magnification factor ($\varepsilon^{n+1}/\varepsilon^n$)
k	Wave number
l_B, S_B	2-D, 3-D body surface boundary
ℓ_f, S_f	2-D, 3-D free surface boundary
$\ell_\infty S_\infty$	2-D, 3-D far-field boundary
$\vec{n}$	Outward unit nomal vector in the domain boundary
$\vec{u}$	Velocity vector of the fluid particle
$\vec{V}$	Velocity vector of the body
$\vec{x}$	Field point vector(x, y, z)

INTRODUCTION

Nonlinear ship motions are comprised of several time scales. The long-time scale problem may be defined as large amplitude oscillations at low frequencies. These motions generate relatively well behaved waves with small to moderate wave slopes. The short-time scale problem is characterized by large relative velocities between hull and water surface where impact, jet-like flows, and breaking waves are common.

Since bow flare impact forces are local and of short duration, numerical schemes can be formulated using finite domain grids concentrated on the vessel's hull and on the near free surface. The attractiveness of the method lies in its use of a restricted domain resulting in a substantial increase in computational efficiency. This is the approach that Troesch and Kang (1988) took when they approximated the free surface boundary condition as an equipotential ($\phi = 0$) surface and when Kang and Troesch (1988) used the complete nonlinear free surface boundary condition with bodies oscillating beneath the free surface. However, when the nonlinear free surface condition and a surface piercing three-dimensional body are used together, instabilities in the time-stepping simulation appeared.

Sawtooth instabilities in free surface calculations of steep water waves were first encountered by Longuet-Higgins and Cokelet (1976). Since that time numerous researchers have presented numerical results that either do not contain the instability for the problems solved, or contain the instability and have to be smoothed and filtered every few time steps. See for example Faltinsen (1977), Vinje and Brevig(1981), Yeung(1982), Dommermuth and Yue(1987), Hong, et al.(1988) or Grilli, et al.(1989). Some have suggested that the instability is purely numerical while others claim that it is a manifestation of the actual physics.

A typical strategy in nonlinear water wave computations is to use a mixed Eulerian-Lagrangian method where the boundary value problem(BVP) is solved at some instant in time and the free surface then time stepped to its new position. The procedure is repeated as desired. In this work, the instantaneous BVP is solved using a Fredholm integral equation of the second kind on the body and a Fredholm integral equation of the first kind on the free surface. The spacial discretization form of the integral equation may be written as :

$$[A] \begin{Bmatrix} \phi, \dfrac{\partial \phi}{\partial n} \\ \dfrac{\partial \phi}{\partial n} \end{Bmatrix} = [B] \begin{Bmatrix} \dfrac{\partial \phi}{\partial n}, \phi \\ \phi \end{Bmatrix} \quad (1)$$

Generally, the vector on the right hand side of the equation is known and the vector on the left hand side is unknown. The bold face potentials and bold face normal derivatives of the potentials denote the free surface elements. The vecotr $\{\phi\}$ on the right side of Eg. (1) is determined through temporal differencing schemes such as staggered implicit/explicit Euler methods or fourth order Runge-Kutta methods. Numerical stability is principally related to the matrices [A] and [B] and the particular differencing scheme selected. These matrices are functions of the boundary geometry, including the bounding boundary at large distances from the body. If the boundaries are changing, as in the nonlinear problem, then the matrices are also functions of time, implying that the stability is time dependent.

Longuet-Higgins and Cokelet (1976) observed "sawtooth instabilities" on the free surface when they followed the time history of space-periodic irrotational surface waves as can be seen in Fig. 1. This sawtooth instability was found when a deep water progressive wave of finite amplitude was marched in time. The authors speculated that this instability was due, partly, to physical reasons and they applied a smoothing technique to remove it.

Faltinsen(1977), in the numerical solution of two-dimensional nonlinear transient problems, found that his solution procedure sometimes became invalid before the surface waves had reached the far-field boundary. To demonstrate this phenomena, he performed the calculation varying the size of the far-field boundary b. In the calculation, he fixed the length of the free surface elements to $\pi a/14$. As shown in Fig. 2, the force grows rapidly in negative values for the case of $b=3.24$. This behavior contrasts with that shown in Fig. 1. In Fig. 1, the error has a sawtooth shape as if a high frequency wave-like error is superposed on the onset flow unlike Fig. 2, where the error appears to grow exponentially. These two figures suggest that numerical errors can ei-

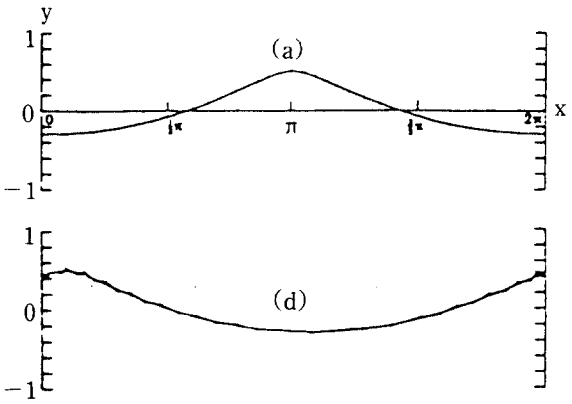

Fig. 1 An example of the sawtooth instability observed by Longuet-Higgins and Cokelet for a steady progressive wave in deep water computed by Pade approximants for Stokes' s series(smooth curve) and the corresponding time-stepped profile(unsmoothed). Number of segments, N=30.
The profiles are compared at times (a) t=0, (d) $t=\pi$. [Longuet-Higgins and Cokelet (1976)].

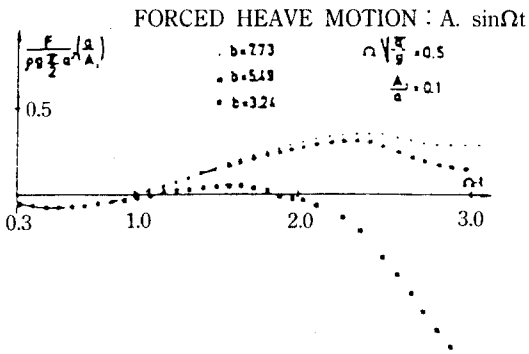

Fig. 2 The vertical force acting on a heaving circular cylinder, an example of the instability observed by Faltinsen. 'b' represents the far-field boundary coordinate, and 'a' the radius of the cylinder. [Faltinsen(1977)]

ther grow exponentially when the error magnification factor is greater that 1.0 and pure real, or grow with changing phase when the error magnification factor is complex and has a modulus greater than 1.0.

The two examples shown in Figs. 1 and 2 suggest that a careful analysis of the numerical schemes used to solve nonlinear free surface flows is warranted. The purpose of this paper, then, is to

- evaluate the numerical stability associated with various forms of the boundary value problem formulation,
- formulate stable time-stepping algorithms,
- demonstrate stable nonlinear calculations, and
- discuss significant modeling problems now that numerical stability can be achieved.

PROBLEM FORMULATION

The coordinate system used in this work is depicted in Fig. 3. The figure represents an infinitely long two-dimensional symmetrical body, or a three-dimensional axisymmetric body, either of which is forced to oscillate vertically on a free surface. The body shape is arbitrary and the body motion can be cyclic or linear with constant velocity in the z direction. The free surface is given by $F=(\vec{x}, t)=0$, where $\vec{x}$ (x, y, z) is the position vector in the right-handed coordinate system. In this system, the z axis is defined as positive upwards, while the y axis represents the calm water level. The origin is at the intersection of the vertical centerline of the body and the undisturbed water surface. The fluid is assumed to be incompressible and inviscid, and the flow is assumed to be irrotational.

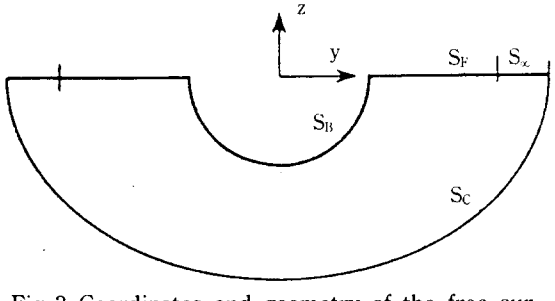

Fig. 3 Coordinates and geometry of the free surface.

The governing equations, boundary conditions, and radiation condition are given as

- Governing equation(Laplace's equation)

$$\nabla^2\phi=0 \text{ in the fluid domain} \cdots\cdots (2)$$

- Kinematic free surface boundary condition

$$\frac{D(z-\eta)}{Dt}=\left(\frac{\partial}{\partial t}+\nabla\phi\cdot\nabla\right)(z-\eta)=0$$
$$on\ z=\eta(x, y, t) \cdots\cdots (3)$$

- Dynamic free surface boundary condition

$$\frac{D\phi}{Dt}=-g\eta+\frac{1}{2}\nabla\phi\cdot\nabla\phi \quad on\ z=\eta(x, y, t)$$
$$\cdots\cdots (4)$$

- Body boundary condition

$$\vec{V}\cdot\vec{n}=\nabla\phi\cdot\vec{n} \quad on\ the\ body\ S_B(x, y, z, t)$$
$$\cdots\cdots (5)$$

- Far-field(radiation) condition

$$\frac{\partial\phi}{\partial n}\rightarrow 0\ as\ |r|\rightarrow\infty \cdots\cdots (6)$$

In the above equations, $\vec{V}$ is the velocity of the body, $\vec{n}$ is the outward unit normal, and $|r|$ is the distance from the origin. The far-field condition is one of the more difficult conditions to apply properly. For the two-dimensional problem, especially, this condition needs to be treated carefully. The far-field truncation effect, properly considered, makes the computational domain finite.

METHOD OF SOLUTION

The method used in this work to solve the boundary value problem of Eqs. 2−6 is called the "mixed Eulerian-Lagrangian method" (Longuet-Higgins and Cokelet(1976)).

The two step approach is adapted here with different numerical schemes in each step. In Step 1, the governing equation using the Boundary Integral Method(BIM) is solved ; and in Step 2, the free surface boundary conditions are satisfied using several different time-stepping schemes.

Green's second identity is employed in the solution of the BIM. The Green function, $G(\vec{x};\vec{\xi})$, is defined as

$$G(\vec{x},\vec{\xi}) = -\frac{1}{2\pi} ln\,|\vec{x}-\vec{\xi}| = -\frac{1}{2\pi} lnr \quad (2-D) \cdots\cdots (7)$$

$$r = \frac{1}{4\pi}\frac{1}{|\vec{x}-\vec{\xi}|} = \frac{1}{4\pi r} \quad (3-D) \cdots\cdots (8)$$

Another solution G* can be obtained by adding any analytic homogeneous solution on the particular solution, Eq. (7) or Eq. (8). One such set of analytic solutions is given as follows

$$G^*(\vec{x};\vec{\xi}) = \frac{1}{2\pi}(lnr + lnc) = \frac{1}{2\pi} lnrc \quad (2-D) \cdots\cdots (9)$$

$$= \frac{1}{4\pi}\left(\frac{1}{r}+\frac{1}{c}\right) \quad (3-D) \cdots\cdots (10)$$

where c is some constant used to normalize the two-dimensional Green function. The integral equations for the velocity potential using G and G* are derived in principal value form as

$$\phi(\vec{x},t) = -\frac{1}{\pi}\int\left\{\phi(\vec{\xi},t)\frac{\vec{n}(\vec{\xi})\cdot(\vec{x}-\vec{\xi})}{|\vec{x}-\vec{\xi}|^2} + \frac{\partial\phi}{\partial n}(\vec{\xi},t) ln\,|\vec{x}-\vec{\xi}|\right\} dl \cdots\cdots (11)$$

or

$$\phi(\vec{x},t) = -\frac{1}{\pi}\int\left\{\phi(\vec{\xi},t)\frac{\vec{n}(\vec{\xi})\cdot(\vec{x}-\vec{\xi})}{|\vec{x}-\vec{\xi}|^2} + \frac{\partial\phi}{\partial n}(\vec{\xi},t) lnc\,|\vec{x}-\vec{\xi}|\right\} dl \cdots\cdots (12)$$

in two-dimensions and in three dimensions as

$$\phi(\vec{x},t) = -\frac{1}{2\pi}\iint\left\{\phi(\vec{\xi},t)\frac{\vec{n}(\vec{\xi})\cdot(\vec{x}-\vec{\xi})}{|\vec{x}-\vec{\xi}|^3} - \frac{\partial\phi}{\partial n}(\vec{\xi},t)\frac{1}{|\vec{x}-\vec{\xi}|^3}\right\} ds \cdots\cdots (13)$$

or

$$\phi(\vec{x},t) = -\frac{1}{2\pi}\iint\left\{\phi(\vec{\xi},t)\frac{\vec{n}(\vec{\xi})\cdot(\vec{x}-\vec{\xi})}{|\vec{x}-\vec{\xi}|^3} - \frac{\partial\phi}{\partial n}(\vec{\xi},t)\left(\frac{1}{|\vec{x}-\vec{\xi}|^3}+\frac{1}{c}\right)\right\} ds \cdots\cdots (14)$$

where $\vec{x}$ and $\vec{\xi} \in$ S, and $\vec{n}$ is an outward unit normal vector.

Two different boundary types are considered here : the near-field closed boundary problem and the far-field open boundary problem. For the near-field closed boundary problem, $S = S_B + S_F + S_C$ where S_C is in the near-field and comprises of the bounding sides and bottom. Either the potential or its normal derivative is given on all surfaces. For the far-field open boundary problem, $S = S_B + S_F + S_\infty + S_C$. The potential takes the form of a dipole on S_∞ and is assumed to be zero on S_C, the closing contour at infinity.

Once the solution to the above equations are found in the fluid domain, the normal derivatives of the potentials on the free surface and the potentials on the body surface are obtained. With this information, the two free surface boundary conditions are stepped in time to determine the new location of the free surface and estimate the potential on that new surface. For the time stepping algorithms in this work, three different Euler methods are chosen ; specifically the explicit,

implicit-like, and implicit Euler methods. Two different fourth-order Runge-Kutta methods are also selected which are the explicit and implicit-like methods.

The various Euler difference approximations for the linearized version of Eqs. 3 and 4, the free surface boundary conditions, are shown below :

- Explicit scheme

$$\phi^{n+1}-2\phi^{n}+\phi^{n-1}=-g(\Delta t)^{2}\phi_{z}^{n-1}, \quad \cdots\cdots\cdots (15)$$

- Implicit-like scheme

$$\phi^{n+1}-2\phi^{n}+\phi^{n-1}=-g(\Delta t)^{2}\phi_{z}^{n} \quad \cdots\cdots\cdots (16)$$

- Implicit scheme

$$\phi^{n+1}-2\phi^{n}+\phi^{n-1}=-g(\Delta t)^{2}\phi_{z}^{n+1} \quad \cdots\cdots\cdots (17)$$

where the superscripts n−1, n, and n+1 represent the values of the potential or its z-derivative at the different time steps. Appendix C of Park(1992) derives the general form of the fourth-order Runge-Kutta algorithm and its discretized forms for the explicit and implicit-like methods.

To apply the free surface boundary condition in the Lagrangian step of the two-step method, the unknown ϕ_n^n on the free surface is calculated using the Boundary Integral Method(BIM), Eqs. (11)−(14). Discretizing the surface with panels (3−D) or line segments (2−D), the potential ϕ at the ith panel or segment is approximated in generic form as ;

$$\phi_i(\vec{\xi}) \cong -\Sigma\left\{\phi_j\int_{\Delta s_j}\frac{\partial G_{ij}}{\partial n_j}dl_j-\left(\frac{\partial\phi}{\partial n}\right)_j\int_{\Delta s_j}G_{ij}dl_j\right\} \quad \cdots\cdots (18)$$

where ϕ_j : known on the free surface

$\dfrac{\partial\phi_j}{\partial n_j}$: unknown on the free surface

and

ϕ_j *or* $\left(\dfrac{\partial\phi}{\partial n}\right)_j$: one is known and the other is unknown on the remaining surfaces

For the linear problem, $\dfrac{\partial\Phi}{\partial n}\rightarrow\dfrac{\partial\Phi}{\partial z}$ on the free surface.

In matrix form, Eq. (18) can be expressed as

$$[A_{ij}]\begin{Bmatrix}\vdots\\ \dfrac{\partial\Phi}{\partial n}\end{Bmatrix}=[B_{ij}]\begin{Bmatrix}\vdots\\ \Phi\end{Bmatrix}$$

or

$$\begin{Bmatrix}\vdots\\ \dfrac{\partial\Phi}{\partial n}\end{Bmatrix}=[C_{ij}]\begin{Bmatrix}\vdots\\ \Phi\end{Bmatrix}=\begin{bmatrix}[C^{1}]&[C^{2}]\\ [C^{3}]&[C^{*}]\end{bmatrix}\begin{Bmatrix}\vdots\\ \Phi\end{Bmatrix} \quad \cdots\cdots (19)$$

where the first m entries in the left-hand column are the unknown potential or unknown normal derivative values on the bottom boundary, body boundary, and the far-field boundary and the rest of the entries in the left-hand column are the unknown normal derivatives of the potential on the free surface. The [C] matrix is the multiplication of the $[A]^{-1}$ and the [B] matrices (i. e. $[C]=[A]^{-1}[B]$).

A subset of the above matrices is made by retaining only the terms needed to complete the time step on the free surface :

$$\begin{aligned}\left\{\frac{\partial\Phi}{\partial n}\right\}&=[[C^{3}]\,[C^{*}]]\begin{Bmatrix}\vdots\\ \Phi\end{Bmatrix}\\&=[C^{2}]\left\{\frac{\partial\Phi}{\partial n}\ or\ \phi\right\}+[C^{*}]\{\phi\}\\&=\sum_{j=f.s.}^{N}C^{*}_{ij}\phi_j+\sum_{j=non\,f.s.}C^{2}_{ij}\left(\left(\frac{\partial\phi}{\partial n}\right)_j\ or\ \phi_j\right)\\&\equiv[C^{*}]\{\phi\}+\{f\}\end{aligned} \quad \cdots\cdots (20)$$

where $[C^{*}]$ is the subset of the influence coefficient matrix [C] which is related to the free surface only. C^{*}_{ij} is the influence coefficient of the

jth free surface panel to the ith free surface panel. The vector {f} is the multiplication of C_{ij}^3 and the known values of ϕ_j or ϕ_{nj} on all surfaces except the free surface. In this way, the vector acts as a forcing function and consequently does not play a role in determining the linear stability characteristics. This summation form, Eq. (20), is substituted to the Eqs. (15)−(17) to study the numerical stability characteristics of the different time stepping schemes.

As an example of the matrix formulation, if ϕ_n is given and ϕ is unknown on the boundaries excluding the free surface, $[A_{ij}]$ and $[B_{ij}]$ then become

$$[A_{ij}]\begin{Bmatrix}\phi\\ \partial\phi/\partial n\end{Bmatrix}=\begin{bmatrix}\frac{1}{2}I_{ij}+\int_{\Delta_{sj}}\frac{\partial G_{ij}}{\partial n}dl_j & -\int_{\Delta_{sj}}G_{ij}dl_j\end{bmatrix}\begin{Bmatrix}\phi\\ \partial\phi/\partial n\end{Bmatrix} \quad \cdots\cdots (21)$$

$$[B_{ij}]\begin{Bmatrix}\partial\phi/\partial n\\ \phi\end{Bmatrix}=\begin{bmatrix}\int_{\Delta_{sj}}G_{ij}dl_j & \frac{1}{2}I_{ij}-\int_{\Delta_{sj}}\frac{\partial G_{ij}}{\partial n}dl_j\end{bmatrix}\begin{Bmatrix}\partial\phi/\partial n\\ \phi\end{Bmatrix} \quad \cdots\cdots (22)$$

where I_{ij} is the identity matrix.

STABILITY ANALYSIS AND ITS IMPLICATIONS

Background

The BIM and finite difference equations described previously will not necesarily converge to the solution of the governing equations. Questions about error propagation and convergence should be answered prior to extensive program use.

Similar to Longuet-Higgins and Cokelet(1976), Baker et al. (1982) also encountered a numerical instability when the local waves were steep. They used a smoothing operator to reduce the effect of the instability. They also found that this instability was reduced remarkably by the use of a dipole distribution rather than a vortex distribution. There are other researchers who observed no such numerical instability. The instability was apparently removed by Roberts(1983) in his analysis of a body-wave interaction problem using Fourier spectral representations for the position and potential of a free shear layer. The modeling was accomplished by a simple modification of the highest (even) Fourier mode. This method of instability removal was also reported by Dold and Peregrine(1984) extending the idea of Vinje and Brevig(1981) with the addition of the higher time derivatives of the complex potential in the Eulerian step. Using the resulting time integration scheme, they found no apparent short-wavelength instability. Another numerically stable scheme was given by Casulli and Cheng(1990) in their discussion of the stability and error analysis for some finite difference methods of the one-dimensional shallow water equations which consist of a system of quasi-linear hyperbolic equations. They showed that the explicit Eulerian-Lagrangian method with fixed grid is unconditionally stable when the Courant-Isaacson-Rees method is used as a time-stepping scheme.

Dommermuth and Yue (1986) and Dommermuth et al. (1988) claimed that the instabilities are not physical but closely related to the accuracy of the velocity calculation for the free surface particles. They postulated that when the mixed Eulerian-Lagrangian scheme is used, the high-wavenumber instability is caused mainly by the concentration of Lagrangian markers in the region of higher gradients. This concentration of the markers, they said, caused a local Courant condition to be inevitably violated for a fixed time step as the waves steepened. They developed a regridding algorithm wherein a new set of equally spaced Lagrangian points on the free surface is

created each time step. This regridding algorithm has the disadvantage of the loss of resolution near the region of high velocity gradients where Lagrangian points would otherwise concentrate. Considering another source, Kang(1988) speculated that the numerical error at the intersection point propagates and could generate saw-tooth instabilities.

Few researchers have actually established stability criteria for water wave problems. Yeung (1982) investigated the stability criteria using a *simplified* von Neumann analysis. He assumed ϕ (x, y, nΔt) to be of the form ϕ^{ikx+ky} where k is a wave number, thus $\phi_y^n = k^n$. His calculation for the numerical stability criteria is simple and easy to follow. However, his stability criteria is independent of the panel length Δx and independent of the various boundary conditions.

Dommermuth et al. (1988) derived the numerical stability criteria using a "linearized von Neumann stability analysis." They also assumed $\phi_y^n = k\phi^n$. By this assumption and a Taylor-series expansion, they found the stability criteria for the explicit fourth-order Runge-Kutta scheme and the fourth-order multi-step Adams-Bashforth-Moulton predictor-corrector(ABM4) scheme. However, by assuming that the normal derivative of the potential on the free surface is proportional to the potential, the stability will be independent of the BIM algorithm. As will be demonstrated in the example sections, the stability criteria determined in this manner is neither an upper nor lower bound.

Two different types of traditional stability analysis will be discussed here(Richtmyer and Morton(1967) and Anderson et al. (1984)). The various methods will be illustrated using the simpler Euler difference approximations, Eqs. (15)－(17). The fourth-order Runge-Kutta methods require a considerable amount of algebraic manipulation and the reader is referred to Park(1992) for details.

von Neumann Stability Analysis

The von Neumann method is well known in the literature. Briefly, the numerical solution is considered to be composed of the exact value and an error. The error, $\varepsilon(\vec{x}, t)$, can be assumed to be written as a series of sine and cosine terms. The ratio between the error at the nth time step and the error at the $(n+1)$th time step is defined as the magnification factor, G. The magnification factor $G(=\varepsilon_j^{n+1}/\varepsilon_j^n)$ for the jth point in the computational grid should be less than 1 in magnitude for the numerical algorithm to be stable. The analysis is only approximate since it does not include the effects of the boundaries. The method's chief attributes are its relative simplicity of implementation and its ability to estimate stability characteristics of individual surface elements. By examining the stability of separate panels, strategies can be developed for variable surface discretizations.

For the free surface problem then, the potential ϕ is considered to be composed of an exact value, ϕ_{exact}, and the numerical error, $\varepsilon(\vec{x}, t)$, The numerical error can be expressed as a Fourier series expansion :

$$\phi = \phi_{exact} + \varepsilon(\vec{x}, t) \quad \cdots\cdots (23)$$

where

$$\varepsilon(\vec{x}, t) = \sum_{m=1}^{\infty} b_m(t) e^{ikmx} = \sum_{m=1}^{\infty} e^{at} e^{ikmx} \quad \cdots\cdots (24)$$

and

$$\varepsilon_j^n = e^{an\Delta t} e^{ikmj\Delta x} \quad \cdots\cdots (25)$$

'a' may be complex but k_m is real.

Applying Eqs. (23)－(25) to the linearized free surface boundary conditions using the various Euler schemes results in

$$\phi^{n+1} - 2\phi^n + \phi^{n+1} = -g(\Delta t)^2 \phi_z^\gamma \quad \cdots\cdots (26)$$

$\gamma=n-1$ for the explicit scheme

where $\gamma=n$ for the implicit-like scheme.

$\gamma=n+1$ for the implicit scheme

The potential derivative ϕ_z^γ on the free surface (i.e. the right-hand side of Eq. (26) is obtained through the application of the BIM in Eq. (20) such as :

$$\{\phi_{zi}\}^\gamma=[C^*]\{\phi_j\}^\gamma+\{f_i\}^\gamma \quad \cdots\cdots (27)$$

where $\phi_j^\gamma=\phi_{jexact}^\gamma+\varepsilon_j^\gamma$, $\{\phi_{zi}\}^\gamma$ is the potential derivative of the ith panel on the free surface at the $n-1$, n, *or* $n+1$ time step and $[C^*]$ is the submatrix related to the free surface potential $\{\phi_i\}^\gamma$. The submatrix $[C^3]$ forms the equivalent of an external exciting function $\{f\}^\gamma$ through the multiplication of known values and consequently does not affect the linear stability analysis. Substituting Eqs. (23)−(25) into Eq. (26) and cancelling common terms yields the equation for the magnification factor $G(=\varepsilon_j^{n+1}/\varepsilon_j^n)$:

$G^2-2G+(1-\alpha)=0$ (Explicit scheme)

$G^2-(2+\alpha)G+1=0$ (Implicit-like scheme)

$(1-\alpha)G^2-2G+1=0$ (Implicit scheme)

where α is a function of discretized panel length, Δx, time-step size, Δt, and the Green function constant, c. The solution of the quadratic equation for the magnification factor G above has two roots. These two roots can have pure real values or complex values and the moduli of the roots are associated with the following stability characteristics :

If $|G|>1$, then the time stepping algorithm is unstable.

If $|G|=1$, then the time stepping algorithm is neutrally stable.

If $|G|<1$, then the time stepping algorithm is stable.

The von Neumann numerical stability analysis of the linearized free surface boundary conditions can also be applied to the fourth-order Runge-Kutta Explicit scheme. See Park(1992) for details.

Matrix Stability Analysis

The disadvantage of von Neumann's approach is that it does not directly include the effects of the boundaries, and therefore gives only approximate stability criteria. A more general, but more computationally intensive way to establish stability criteria is the Matrix Method(Richtmyer and Morton(1967) and Anderson et al. (1984)). The method will now be applied to the two linear free surface boundary conditions :

$$\frac{\partial\phi}{\partial t}=-g\eta \quad on \quad z=0 \quad \cdots\cdots (28)$$

$$\frac{\partial\eta}{\partial t}=\phi_z=[C^*]\phi+f$$

The discretized system of the two boundary conditions can be written in general matrix form

$$\begin{Bmatrix}\phi\\ \vdots\\ \eta\\ \vdots\end{Bmatrix}^{n+1}=\begin{bmatrix}\\ D_{ij}\\ \\ \end{bmatrix}\begin{Bmatrix}\phi\\ \vdots\\ \eta\\ \vdots\end{Bmatrix}^{n}+\begin{Bmatrix}0\\ \vdots\\ f\\ \vdots\end{Bmatrix}^{n} \quad \cdots\cdots (29)$$

where $[D]$ is a $(2N\times 2N)$ matrix and N represents the number of panels on the free surface. If any one of the absolute values of the 2^*N eigenvalues of $[D]$ is larger than 1, then the marching scheme is unstable (See Richtmyer and Morton(1967) and Anderson et al.(1984). The formation of the $[D]$ matrix is decided according to the choice of numerical schemes. It follows that the eigenvalues of the $[D]$ matrix have a meaning very similar to that of the roots of the magnification factor G in the von Neumann analysis. As examples, consider the explicit and implicit-like Euler schemes :

The difference equations using the explicit Euler scheme is as follows :

$$\phi_i^{n+1}=\phi_i^n-g\Delta t\eta_i^n$$

$$\eta_i^{n+1}=\eta_i^n+\Delta t\sum_{j=1}^{N}C_{ij}^*\phi_j^n+f_i^n \quad \cdots\cdots(30)$$

or combined into matrix form :

$$\begin{Bmatrix}\phi\\ \vdots\\ \eta\\ \vdots\end{Bmatrix}^{n+1}=\left[\begin{array}{cc|cc}1 & & 0 & -g\Delta t\\ & 0 & & 0\\ \hline & \Delta tC^* & 1 & \\ & & & 0\end{array}\right]\begin{Bmatrix}\phi\\ \vdots\\ \eta\\ \vdots\end{Bmatrix}^{n}+\begin{Bmatrix}0\\ \vdots\\ f\\ \vdots\end{Bmatrix}^{n} \quad (31)$$

As can be seen in Eq. (31), the [D] matrix of the explicit Euler scheme is composed of two identity matrices, one $-g\Delta t^*[I]$ matrix, and the $\Delta t^*[C^*]$ matrix, a subset of the [C] matrix.

The difference equations using the implicit-like scheme are as follows :

$$\phi_i^{n+1}=\phi_i^n-g\Delta t\eta_i^{n+1}$$

$$\eta_i^{n+1}=\eta_i^n+\Delta t\sum_{j=1}^{N}C_{ij}^*\phi_j^n+f_i^n \quad \cdots\cdots(32)$$

with a matrix representation of

$$\left[\begin{array}{cc|cc}1 & & 0 & g\Delta t\\ & 0 & & 0\\ \hline & & 1 & \\ & \Delta tC^* & & 0\end{array}\right]\begin{Bmatrix}\phi\\ \vdots\\ \eta\\ \vdots\end{Bmatrix}=\left[\begin{array}{cc|cc}1 & & 0 & 0\\ & 0 & & 0\\ \hline & & 1 & \\ & \Delta tC^* & & 0\end{array}\right]\begin{Bmatrix}\phi\\ \vdots\\ \eta\\ \vdots\end{Bmatrix}^{n}+\begin{Bmatrix}0\\ \vdots\\ f\\ \vdots\end{Bmatrix}^{n} \quad \cdots\cdots(33)$$

To construct the [D] matrix of Eq. (29) using the implicit-like Euler scheme, the inverse of the matrix on the left-hand side of the above equation should be multiplied on both sides. As with the explicit method, the [D] matrix includes the [C*] matrix.

The fourth-order Runge-Kutta schemes can also be put into matrix from. The detailed procedure for the derivation and formation of the [D] matrix is given in Appendix C of Park(1992).

APPLICATIONS

It is possible to find an analytic solution for the stability region in some very simple cases. Park (1992) derives the closed form expression based upon Eq. (26) for the stability criteria of a *single* free surface panel satisfying the linear free surface boundary conditions. The potential and its normal derivative are known on all other surfaces. This idealized problem is meant as a first step in understanding the complicated behavior associated with more typical free surface problems. When the number of free surface panels is greater than one or when nonlinear boundary conditions are used, the stability criteria must be determined numerically.

In the examples given below, the validity of the method will be demonstrated by comparing estimated stability boundaries with analytical values and the results of numerical simulation thus making the extension to more complex models straightforward. Since it is not possible to obtain an analytic solution for the stability of numerical solutions involving the nonlinear free surface boundary, the stability analysis begins with the linear boundary conditions and linear geometry using the assumption that the nonlinear effect on stability is small in the limit of small wave slope. Within this assumption, the linear stability study becomes the basis for the nonlinear stability analysis. The last example in this section will involve the fully nonlinear free surface conditions with time dependent influence coefficient matrices. This contrasts with the linear calculations, where the influence coefficient matrix does not change during the time interval of interest.

Linear Closed Boundary Problem

The model geometry and the coordinate system are depicted in Fig. 4. The free surface boundary

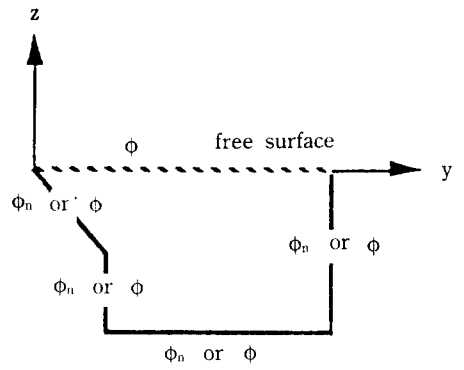

Fig. 4 Model of the closed boundary problem. General polygonal shape

condition is imposed on top and φ or ϕ_n on the other sides. For the purpose of simulation, the initial conditions on the free surface and other boundaries are given as those of plane progressive wave. This may be thought of as the far-field solution to the wave maker problem.

The first example considered will be a square panel with sides 2a. One panel is located on the free surface, one panel on the bottom, and one panel on each side. The geometry of the boundary and its coordinate system is shown in Fig. 5.

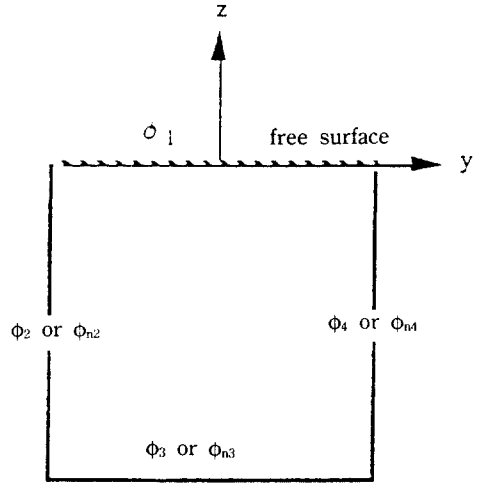

Fig. 5 Geometry of the square panel of the closed boundary problem. The potential φ is given on the top panel and φ or ϕ_n for the other panels.

For ϕ_n given on the side and bottom panels, following Eq. (20) the solution for the potential is given as

$$\phi_1 = A\frac{\partial\phi_1}{\partial n} + B\phi_2 + C\frac{\partial\phi_2}{\partial n} + B\phi_3 - C\frac{\partial\phi_3}{\partial n} + D\phi_4 + E\frac{\partial\phi_4}{\partial n} \quad \cdots\cdots (34)$$

$$\phi_2 = B\phi_1 + C\frac{\partial\phi_1}{\partial n} + A\frac{\partial\phi_2}{\partial n} + D\phi_3 + E\frac{\partial\phi_3}{\partial n} + B\phi_4 + C\frac{\partial\phi_4}{\partial n} \quad \cdots\cdots (35)$$

$$\phi_3 = B\phi_1 + C\frac{\partial\phi_1}{\partial n} + D\phi_2 + E\frac{\partial\phi_2}{\partial n} + A\frac{\partial\phi_3}{\partial n} + B\phi_4 + C\frac{\partial\phi_4}{\partial n} \quad \cdots\cdots (36)$$

$$\phi_4 = D\phi_1 + E\frac{\partial\phi_1}{\partial n} + B\phi_2 + C\frac{\partial\phi_2}{\partial n} + B\phi_3 + C\frac{\partial\phi_3}{\partial n} + A\frac{\partial\phi_4}{\partial n} \quad \cdots\cdots (37)$$

where

$$A = -\frac{2a}{\pi}(\ln ca - 1) \quad \cdots\cdots (38)$$

$$B = \frac{1}{\pi}\tan^{-1}2 \quad \cdots\cdots (39)$$

$$C = \frac{2a}{\pi}\left(\ln\sqrt{5}ac - 1 + \frac{1}{2}\tan^{-1}2\right) \quad \cdots\cdots (40)$$

$$D = \frac{2}{\pi}\tan^{-1}\frac{1}{2} \quad \cdots\cdots (41)$$

$$E = -\frac{2a}{\pi}\tan\left(\ln\sqrt{5}ac - 1 + 2\tan^{-1}\frac{1}{2}\right) \quad \cdots (42)$$

In matrix from for the case of (ϕ_1, ϕ_{n2}, ϕ_{n3}, ϕ_{n4}) known and (ϕ_{n1}, ϕ_2, ϕ_3, ϕ_4) unknown, the equations become :

$$\begin{Bmatrix} \frac{\partial\phi_1}{\partial n} \\ \phi_2 \\ \phi_3 \\ \phi_4 \end{Bmatrix} = [\ C_{ij}\ ] \begin{Bmatrix} \phi_1 \\ \frac{\partial\phi_2}{\partial n} \\ \frac{\partial\phi_3}{\partial n} \\ \frac{\partial\phi_4}{\partial n} \end{Bmatrix} \quad \cdots\cdots (43)$$

where the unknown normal velocity of the free surface element is

$$\frac{\partial \phi_1}{\partial n} = C_{11}\phi_1 + \sum_{j=2}^{4} C_{1j}\phi_{nj} \quad \cdots\cdots (44)$$

and the [C] matrix is the inverse of the (ϕ_{n1}, ϕ_2, ϕ_3, ϕ_4) influence coefficient matrix multiplied by the (ϕ_1, ϕ_{n2}, ϕ_{n3}, ϕ_{n4}) influence coefficient matrix.

Equation (44) is an analytic solution form for ϕ_n on the free surface assuming that the given potential on the free surface and the normal derivatives on the other surfaces are constant over each panel or segment. Recall that for the linearized problem, the term $\Sigma_{j=2}^{4} C_{1j}\phi_{nj}$ of Eq. (44) acts as an exciting force in the stability equation and as such plays no role in determining the stability characteristics.

For the explicit Euler scheme, the free surface difference equation for the closed boundaries becomes

$$\phi_1^{n+2} - 2\phi_1^{n+1} + \phi_1^n = -g(\Delta t)^2\{C_{11}\phi_1^n + \sum_{j=2}^{4} C_{1j}\phi_{nj}^n\} \quad \cdots\cdots (45)$$

Following a von Neumann stability analysis yields the quadratic equation for the magnification factor :

$$G^2 - 2G + 1 = -g(\Delta t)^2 C_{11}$$

or

$$G^2 - 2G + \{+g(\Delta t)^2 C_{11}\} = 0 \quad \cdots\cdots (46)$$

There is no region where $|G| < 1$. Therefore, no stability region exists and the explicit Euler scheme is *unconditionally unstable* for the square panel of the closed boundary problem.

The difference for the implicit-like Euler scheme is

$$\phi_1^{n+2} - 2\phi_1^{n+1} + \phi_1^n = -g(\Delta t)^2\{C_{11}\phi_1^{n+1} + \sum_{j=2}^{4} C_{1j}\phi^{n+1}{}_{nj}\} \quad \cdots\cdots (47)$$

which has the associated quadratic equation for the magnification

$$G^2 - 2G + 1 = -g(\Delta t)^2 C_{11} G$$

or

$$G^2 - \{2 - g(\Delta t)^2 C_{11}\}G + 1 = 0 \quad \cdots\cdots (48)$$

The stability regionis

$$0 < \frac{g(\Delta t)^2}{2} C_{11} < 2 \quad \cdots\cdots (49)$$

Therefore, the implicit-like Euler scheme is *conditionally unstable* in the region where Eq. (49) is satisfied.

The term $1/\Delta x$ appears explicitly in matrix element C_{11}. Define a free surface stability parameter(FSS) as $\frac{\pi g(\Delta t)^2}{\Delta x}$. The equations above represent the case of ϕ given on the free surface and ϕ_n given on the other sides. The approach is quite general and the results for other combinations of ϕ and ϕ_n are shown in Table 1. Clearly, the boundary condition type can play an important role in determining the numerical stability limit.

Table 1. Stability limits of the square panel with different boundary condition types. "Boundary Condition Type" represents the known boundary values on each panel. The implicit-like Euler scheme is used.

Case	*Boundary Condition Type*	*Stability Limit (FSS number)*
1	ϕ_1, ϕ_2, ϕ_3, ϕ_4	*5.47*
2	ϕ_1, ϕ_{n2}, ϕ_3, ϕ_4	*7.18*
3	ϕ_1, ϕ_{n2}, ϕ_3, ϕ_{n4}	*8.14*
4	ϕ_1, ϕ_{n2}, ϕ_{n3}, ϕ_4	*10.70*

Time simulations of a plane progressive wave passing through the square panel are performed for the various ranges of the FSS number and typical results are shown in Figs. 6−9. Fig. 6 is the

condition for a very small FSS number. In this case, the simulation shows both high levels of accuracy with stability. The FSS number is increased to the stability limit to investigate the transition phenomena from a stable to unstable region (Fig. 7). figure 7 shows the sawtooth contamination on the crest and trough of the sine curve. With an incremental increase in the FSS number, (FSS=7.185) the simulation diverges drastically as in Fig. 8. In Fig. 9, the FSS unmber is set to a value of 0.01 a highly stable condition, but the $k\Delta x$ value, where k is the plane progressive wave number, is increased to 2.2. Figure 9 demonstrates that stability does not necessarily guarantee accuracy. With out presenting the details here, Park(1992) has shown that the fully implicit Euler scheme is also *Conditionally stabe* and that the explicit fourth-order Runge-Kutta scheme has approximately double the range of the FSS parameter of the implicit-like Euler scheme.

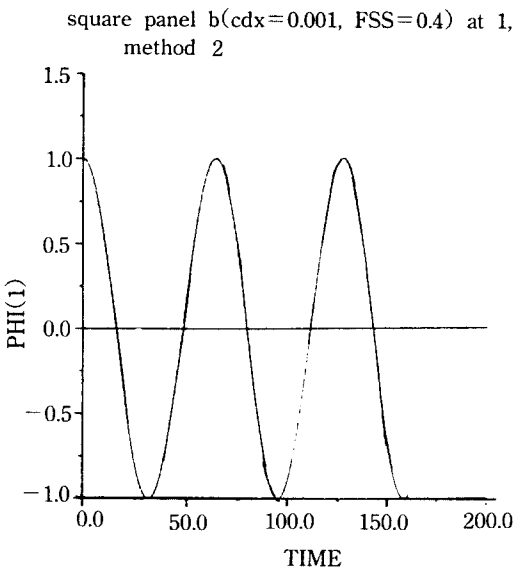

Fig. 6. Time simulation of the square panel. Boundary conditions given as (ϕ_1, ϕ_{n2}, ϕ_3, ϕ_4) with implicit-like Euler scheme for time marching.
FSS number=0.4.

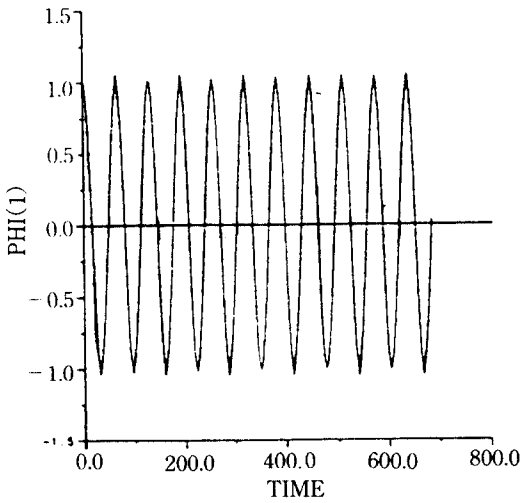

Fig. 7. Time simulation of the square panel. Boundary conditions given as (ϕ_1, ϕ_{n2}, ϕ_3, ϕ_4) with implicit-like Euler scheme for time marching. FSS number=7.180.

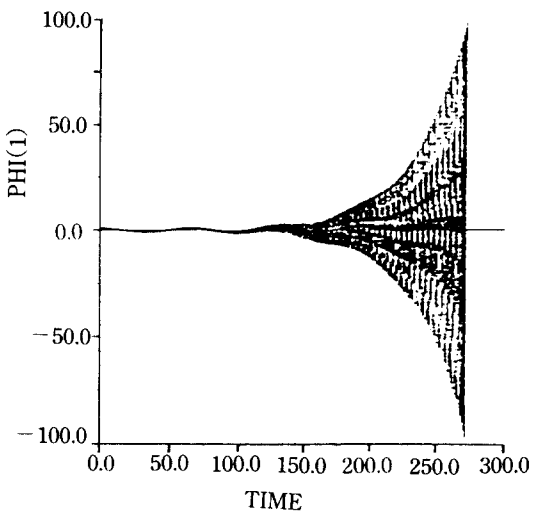

Fig. 8. Time simulation of the square panel. Boundary conditions given as (ϕ_1, ϕ_{n2}, ϕ_3, ϕ_4) with implicit-like Euler scheme for time marching. FSS number=7.185.

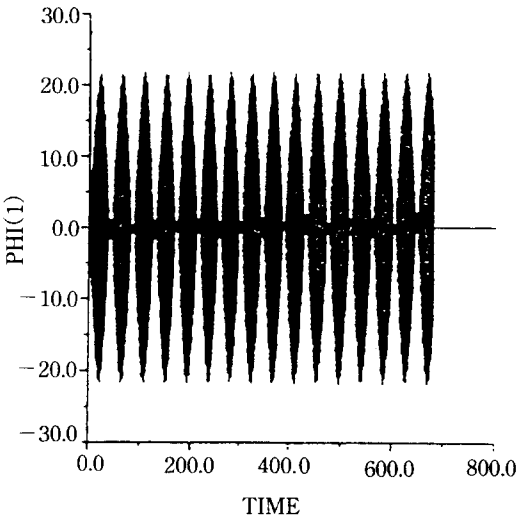

Fig. 9. Time simulation of the square panel. Boundary conditions given as (ϕ_1, ϕ_{n2}, ϕ_3, ϕ_4) with implicit-like Euler scheme for time marching. FSS number=0.01 and kΔx=2.2.

Much of the problem formulation and the resulting mathematical equations are the same for the polygonal domain with N panels on the free surface. The geometry of the domain is shown in Fig. 4. For the explicit Euler shceme, the difference equations are found by substituting Eq. (27) into Eq. (26) to find

$$\phi_j^{n+2}-2\phi_j^{n+1}+\phi_j^n+g(\Delta t)^2\sum_{m=f.s.}^{N}C_{jm}^{*}\phi_m^n = -g(\Delta t)^2\sum_{m=non\,f.s.}C_{jm}^{3}\cdot(\phi_m^n \ or \ \phi_{nm}^n) \cdots (50)$$

Following the von neumann stability analysis, the quadratic form of the magnification factor equation is

$$G_j^2-2G_j+1+g(\Delta t)^2\Big(\sum_{m=f.s.}^{N}C_{jm}^{*}e^{i(m-j)\beta}=0 \cdots\cdots (51)$$

with roots

$$G_j=1\pm\sqrt{-g(\Delta t)^2\Big(\sum_{m=f.s.}^{N}C_{jm}^{*}e^{i(m-j)\beta}} \cdots\cdots (52)$$

where $\beta=k\Delta x$ and k is the wave number of the Fourier component of the error. The magnitude of at least one of the two roots is larger than 1 ($|G|>1$) ; therefore, no region of stability exists. The explicit Euler scheme is *unconditionally unstable* for the multi-panel closed boundary problem, similar to the single-panel closed boundary problem discussed previously.

The implicit-like Euler scheme has the following difference equations for the multi-panel boundary :

$$\phi_j^{n+2}-2\phi_j^{n+1}+g(\Delta t)^2\sum_{m=f.s.}^{N}C_{jm}^{*}\phi_m^{n+1}+\phi_m^n = -g(\Delta t)^2\sum_{m=non\,f.s.}C_{jm}^{3}\cdot(\phi_m^{n+1} \ or \ \phi_{nm}^{n+1}) \cdots\cdots (53)$$

Based upon a von Neumann analysis, the quadratic form of the magnification factor equation is

$$G_j^2-\{2-g(\Delta t)^2\Big(\sum_{m=f.s.}^{N}C_{jm}^{*}e^{i(m-j)\beta}\}G_j+1=0 \cdots\cdots (54)$$

At the(j) panel, the magnification factor G_j is easily shown to be

$$G_j=1-\frac{g(\Delta t)^2}{2}\Big(\sum_{m=f.s.}C_{jm}^{*}e^{i(m-j)\beta}\pm\Big[-\frac{g(\Delta t)^2}{2}\Big(\sum_{m=f.s.}^{N}C_{jm}^{*}e^{i(m-j)\beta}\Big)+\frac{g^2(\Delta t)^4}{2}\Big(\sum_{m=f.s.}^{N}C_{jm}^{*}e^{i(m-j)\beta}\Big)^2\Big]^{1/2} \cdots\cdots (55)$$

the stability region has to be numerically calculated. Therefore, the implicit-like Euler scheme is *conditionally stable* in the region where Eq. (55) is satisfied. Equation(55) can be used to search for the stable region of each panel on the free surface. For each panel, the local maximum FSS number(i.e. the largest FSS number before the calculation becomes unstable) is calculated. The smallest FSS number among the local maximum FSS numbers is taken to be the stability limit for entire free surface. As an example, Table 2 shows the distribution of the maximum FSS numbers along the free surface panels of a right triangular domain. The boundary condition was given as the potential derivatives (ϕ_n) on the lo-

ngest slanted side. On the free surface and on the vertical side, potentials were given as shown on Fig. 10. Forty panels were located on the free surface, nine panels on the vertical side, and forty-one panels on the slanted side. Panels on the free surface are numbered from the right as 51 to the left as 90. Table 2 reveals that the stability limit is greater near both edges and smaller in the middle indicating that the least stable elements are located near the center.

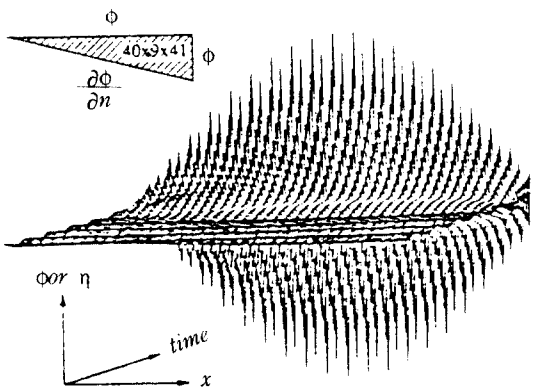

Fig. 10 Free surface simulation for the triangular domain. Boundary conditions given as ϕ on the free surface, ϕ on the vertical boundary, and ϕ_n on the slanted boundary. Implicit-like Euler scheme.
FSS number=4.685, c=1.0

Figure 10 is the time simulation result corresponding to the example of Table 2. The FSS number was fixed at 4.685 which is a stable FSS number for the edges and an unstable FSS number for the middle panels. The figure shows growth in the error of the potential on the middle and the effect propagates to the edges. The matrix method can be used to evaluate the stability of the implicit-like fourth-order Runge-Kutta scheme for the same geometry. Park(1992) calculated that the implicit-like RK-4 algorithm becomes unstable at an FSS number of approximately 5.02.

Table 2. Maximum FSS number along the free surface on the trangular domain. Boundary conditions given as ϕ on the free surface, ϕ on the vertical boundary, and ϕ_n on the slanted boundary. Implicit-like Euler scheme, c=1.0

40*9*41 RIGHT TRIANGLE : (20011) BOUNDARY CONDITION

With Implicit-like Euler scheme

****

panel no. 51 : FSSmax=0.50327953521990E+01
panel no. 52 : FSSmax=0.46935572888574E+01
panel no. 53 : FSSmax=0.46657763639911E+01
panel no. 54 : FSSmax=0.46647364292390E+01
panel no. 55 : FSSmax=0.46654495985777E+01
panel no. 56 : FSSmax=0.46645214740659E+01
panel no. 57 : FSSmax=0.46653739332471E+01
panel no. 58 : FSSmax=0.46646326873699E+01
panel no. 58 : FSSmax=0.46652636309610E+01
panel no. 60 : FSSmax=0.46647314596044E+01
panel no. 61 : FSSmax=0.46651773814673E+01
panel no. 62 : FSSmax=0.46648066659406E+01
panel no. 63 : FSSmax=0.46651111359308E+01
panel no. 64 : FSSmax=0.46648658877095E+01
panel no. 65 : FSSmax=0.46650572343171E+01
panel no. 66 : FSSmax=0.46649158698483E+01
panel no. 67 : FSSmax=0.46650099898935E+01
panel no. 68 : FSSmax=0.46649613650187E+01
panel no. 69 : FSSmax=0.46649653730346E+01
panel no. 70 : FSSmax=0.46650058975132E+01
panel no. 71 : FSSmax=0.46649201553847E+01
panel no. 72 : FSSmax=0.46650525951354E+01
panel no. 73 : FSSmax=0.46648711199720E+01
panel no. 74 : FSSmax=0.46651049612333E+01
panel no. 75 : FSSmax=0.46648142506205E+01
panel no. 76 : FSSmax=0.46651677654242E+01
panel no. 77 : FSSmax=0.46647435023243E+01
panel no. 78 : FSSmax=0.46652480804577E+01
panel no. 79 : FSSmax=0.46646470102447E+01
panel no. 80 : FSSmax=0.46653522313344E+01
panel no. 81 : FSSmax=0.46644836160268E+01
panel no. 82 : FSSmax=0.46654442871698E+01
panel no. 83 : FSSmax=0.46641023690973E+01
panel no. 84 : FSSmax=0.46656975490966E+01
panel no. 85 : FSSmax=0.46661354209918E+01
panel no. 86 : FSSmax=0.46850759928442E+01
panel no. 87 : FSSmax=0.47774251888542E+01
panel no. 88 : FSSmax=0.52561249903248E+01
panel no. 89 : FSSmax=0.72196326036770E+01
panel no. 90 : FSSmax=0.12954511994784E+01

Linear Open Boundary Proglem

The model geometry and the coordinate system for the linear open boundary are depicted in Fig. 3. The fluid is bounded by the free surface S_F and S_∞, by the rigid body S_B, and by the bottom and far-away contour S_C. The surface S changes to a line contour in the two dimensional problem. Following Faltinsen(1977) for the two-dimensional case and Kang(1988) for three-dimensional axisymmetric case, the behavior of the potential ϕ in the far-field is considered to be the same as the value of a vertical dipole at the origin. The strength of the vertical dipole is determined through matching it to the value of ϕ_z on the last panel at the truncation boundary. The effects of the normalization constant c in the modified Green function(i. e. G^*) and the truncation boundary are included and the accuracy of the numerical scheme has been checked with the continuity equation(conservation of mass).

This Investigation is essentially numerical. The complexity of the boundary value problem, including boundory conditions and time-stepping algorithms, ristricts stability analysis to numerical studies. The matrix method, Eqs. (29)~(33), is used to determine the stability characteristics.

Table 3 shows the numerical stability results as a function of the parameters c, the modified Green function constant, and the FSS number. This analysis was performed with 10 panels on the half wedge-type body which has 45 degree slope(i. e. 45 degree wedge half angle) and 20 panels on the free surface. The explicit fourth-order Runge-Kutta scheme was used. The numbers in the table represent the maximum modulus of the eigenvalues in the matrix stability analysis, so the condition which has a value larger than 1 is unstable and the condition which has the value less than or equal to 1 is stable. The stable region is observed by varying c from 1.0 to 0.1 to 0.01. The results suggest that the proper manipulation of c in the modified two-dimensional Green function controls the numerical stability for this linearized problem. The possibility of stability control for other problems and other numerical schemes is worthy of further investigation.

Table 3. Magnitude of maximum eigenvalues associated with the forced oscillation, far-field open boundary problem. 45 degree half angle, wedge-shape two-dimensional body on the free surface with 10 panels on the body, 20 on the free surface. Explicit fourth-order Runge-Kutta scheme. (r) and (c) denote real or complex eigenvalues respectively. w/ : with truncation effect, w/o : without truncation effect.

c	0.01		0.10		1.00	
FSS	w/	w/o	w/	w/o	w/	w/o
1.0	1.0(c)	1.0(c)	1.144(r)	0.9999(c)	1.067(r)	1.117(r)
2.0	1.0(c)	1.0(c)	1.209(r)	0.9999(c)	1.096 (r)	1.169(r)
3.0	1.0(c)	1.0(c)	1.262(r)	0.9999(c)	1.122 (r)	1.211(r)
4.0	1.0(c)	1.0(c)	1.308(r)	0.9999(c)	1.138 (r)	1.247(r)
5.0	1.0(c)	1.0(c)	1.350(r)	0.9999(c)	1.156 (r)	1.280(r)
9.0				0.9994(c)		
10.0				1.255 (c)		

The effect of the treatment of the truncation boundary on the stability is also demonstrated. Complex eigenvalues referenced to the unit circle are shown in Figs. 11 and 12. As can be seen in Table 3 and Fig. 11, the maximum eigenvalue of 1.144 is pure real while Fig. 12 shows the maximum eigenvalue of 1.255 is complex. Figure 11 implies a diverging error with fluctuation while Fig. 12 implies an exponentially diverging error. A simulation is shown in Fig. 13 for the condition shown in Fig. 11. In these two figures, the truncation effect was included following Faltinsen's far-field model and exhibits instabilities similar to

the type of instability shown in the Introduction, Fig. 2.

Eigenvalues of test case for the open -boundary problem

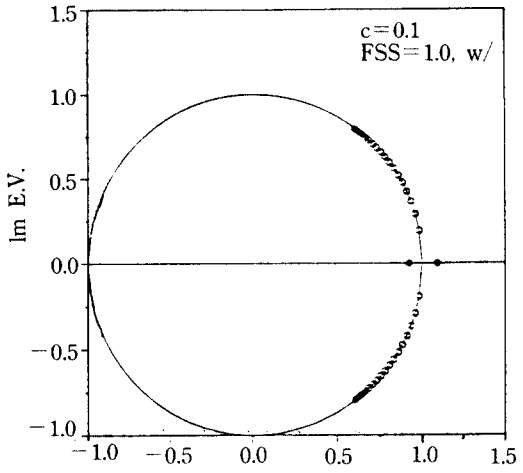

Fig. 11. Eigenvalues of the forced oscillation, far-field open boundary problem 45 degree half angle, wedge-shaped two-dimensional body on the free surface with 10 panels on the body, 20 on the free surface. Explicit fourth-order Runge-Kutta scheme. c=0.1, 'o' represents the eigenvalues for FSS number=1.0 with the truncation effect.

The effects of three dimensionality and increased panel numbers on the free surface are examined next. Consider a cone shaped surface with a 45 degree half angle. The three dimensional modified Green function (Eqs. (12) and (14)) is used to formulate the integral equation of the BIM. Due to the axisymmetric shape, the theta integration is performed in closed form reducing the physical dimensions by one. The influence coefficients in the [A] and [B] matrices will reflect this integration and produce changes in the stability characteristics of the problem. As a far-field closure, the truncation effect is considered

Eigenvalues of test cases

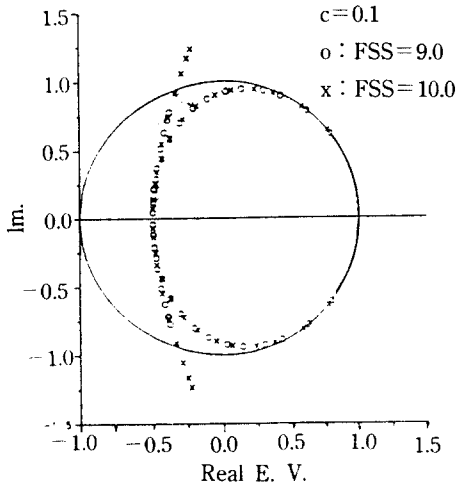

Fig. 12 Eigenvalues of the forced oscillation, far-field open boundary problem. 45 degree half angle, wedge-shaped two-dimensional body on the free surface with 10 panels on the body, 20 on the free surface. Explicit fourth-order Runge-Kutta scheme. c=0.1, 'o' represents the eigenvalues for FSS number=9.0 and 'x' for FSS number=10.0 both without the truncation effect.

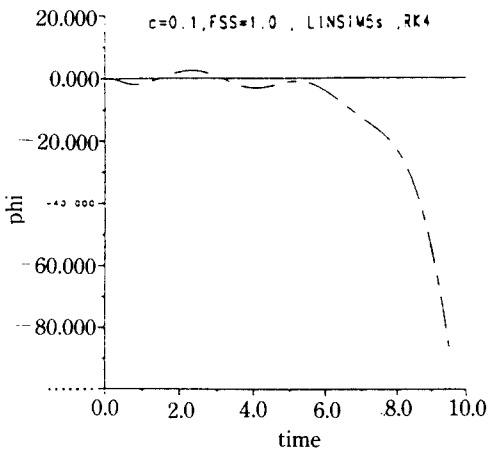

Fig. 13 Time simulation for the forced oscillation, far-field open boundary problem. 45 degree half angle, wedge-shaped two-dimensional body on the free surface with 10 panels on the body, 20 on the free surface. Explicit fourth-order Runge-Kutta scheme. c=0.1, FSS number=1.0 with the truncation effect.

by the method of Kang(1988) where the far-field behavior is approximated by a single vertical dipole located at the origin.

Tables 4 and 5 show the numerical stability results for two-dimensional and three-dimensional axisymmetric cases with similar conditions (10 panels on the half-body, go panels on the free surface, and the explicit fourth-order Runge-Kutta scheme). From the results presented here, it is found that the far-field closure consideration is not a major factor for the stability analysis of the three-dimensional axisymmetric case. In two-dimensions, as already shown, the stability region can be altered by the far-field closure condition. For the two dimensional case, this appears to be quite reasonable since wave energy propagated from the body is not dispersed radially in the far-field. The proper closure method then becomes much more important than in the three-dimensional case.

The effect of the Green function constant is also very weak in three-dimensions. For two dimensions, c should be less than 0.02 for the computation to be stable. In three dimensions, the stability characteristics, through four significant figures, were unaffected by c. This suggests that little is to be gained by using the modified Green function(i. e. Eq. (10)) in three dimensions.

In addition to the examples considered here, Park(1992) also investigated other time-stepping schemes. Several runs with implicit-like fourth-order Runge-kutta schemes and Kang's fourth-order Runge-Kutta scheme(Kang(1988)) were performed and *no stable regions were found*. In the implicit-like Runge-Kutta scheme, the modulus of the maximum eigenvalues converged to 1.0 in the limit as the FSS number went to zero. Hence, for the very smally numbered range of the FSS number near 0.0, an implicit-like method may also be admissible in the calculation of the impact problem for short-time spans.

Table 4. Magnitude of maximum eigenvalues associated with the forced oscillation, far-field open boundary problem. 45 degree half angle, wedge-shaped *two-dimensional body* on the free surface with 10 panels on the body, 90 on the free surface. Explicit fourth-order Runge-Kutta scheme. (r) and (c) denote real or complex eigenvalues respectively. w/ : with truncation effect, w/o : without truncation effect.

c	0.01		0.02		0.10		1.00	
FSS	w/	w/o	w/	w/o	w/	w/o	w/	w/0
1.0	1.0	1.0	1.127	1.0(c)	1.041	1.086	1.027(r)	1.043
2.0	.0	1.0	1.184	1.0(c)	1.058	1.124	1.038(r)	1.062
3.0	1.0	1.0	1.230	1.0(c)	1.072	1.154	1.046(r)	1.076
4.0	.0	1.0	1.270	1.0(c)	1.083	1.179	1.054(r)	1.088
5.0	.0	1.0	1.307	1.0(c)	1.093	1.203	1.060(r)	1.099
9.0				1.0(c)				
10.0				1.275(c)				

Table 5. Magnitude of maximum eigenvalues associated with the forced oscillation, far-field open boundary problem. 45 degree half angle, cone-shaped *three-dimensional axisymmetric body* on the free surface with 10 panels on the body, 90 on the free surface. Explicit fourth-order Runge-Kutta scheme. All values were complex(c) eigenvalues. w/ : with truncation effect, w/o : without truncation effect.

l/c	10.0		1.0		0.01		0.00	
FSS	w/	w/o	w/	w/o	w/	w/o	w/	w/0
1.0	1.0	1.0	1.0	1.0	1.0	1.0	1.0	1.0
9.33	1.0	1.0	1.0	1.0	1.0	1.0	1.0	1.0
10.0	1.275	1.275	1.275	1.275	1.275	1.275	1.275	1.275
11.0	1.755	1.755	1.755	1.755	1.755	1.755	1.755	1.755
12.0	2.307	2.307	2.307	2.307	2.307	2.307	2.307	2.307

The linear stability analysis discussed in this chapter has laid the foundation for understanding

the nonlinear calculations. Effects on numerical stability, such as time differencing schemes, boundary formulations and temporal and spatial discretizations have been investigated. While these findings may have to be refined in the cases of steep, breaking waves or jets due to impact, the next chapter will demonstrate that the linear results are valid for moderately nonlinear wave calculations.

Nonlinear Open Boundary Problems

With the basic theory of the linear numerical stability analysis firmly established, the nonlinear numerical stability analysis for the forced oscillation problem can be examined. Most of the problem solving procedures are the same as that described above except that the free surface boundary conditions are now nonlinear and the body boundary condition is satisfied on the exact body surface. The Boundary Integral Method(BIM) is used in solving Laplace's equation and the fourth-order Runge-Kutta schemes are used for time-stepping the nonlinear free surface conditions. At each time step, the body and the free surface shape are regridded using modified Lagrangian polynomials (i. e. non-uniform parametric blended Lagrangian polynomials). For the fourth-order Runge-Kutta schemes, the influence coefficient matrix may or may not be updated during the intermediate steps depending upon the method used.

Park(1992) describes a number of concerns related to the nonlinear body-wave interaction problem. The stability and closure issues of the previously discussed linear problem are still present. With nonlinear boundary conditions, though, a number of other factors must also be considered, including the body-free surface intersection curve and the effects associated with any regridding algorithm.

At the intersection point, the body boundary condition, usually given as a Neumann type, meets the free surface boundary condition, usually a Dirichlet type. The confluence of these two boundary conditions causes a weak singularity in the integral equation. This weak signularity on the intersection point has a global influence and causes numerical difficulties for the nonlinear problem. For the results presented here, the position and the potential of the computational surface is calculated at the center of the panel in the BIM. By locating the control point at the center of the panel, the logarithmic singularity at the intersection point is removed. However, locating the control point at the panel center introduces the difficulty of tracing the intersection point where a kinematic continuity is satisfied. Here the tangential velocity of the intersection point is determined by the modified Lagrangian polynomial interpolation scheme and the normal velocity of the intersection point is determined via the body boundary condition to be the same as the normal velocity of the body(Park 1992).

After each time step, a new location of the body-wave intersection point is also calculated to get the wetted body length. Starting from the new body-wave intersection point, the total arc length of the free surface is calculated. The free surface is then regridded to have constant panel lengths. For the portion where the high gradient potential exists, more panels are allocated to prevent the possible loss of accuracy due to the regridding algorithm. After the regridding procedure, the new location of the control points and the potential values on the new control points of the free surface are recalculated. To investigate the numerical stability behavior relative to a given FSS number, the time step Δt is tuned to keep the FSS number constant according to the modified panel length Δx, at every time step.

Since a fully nonlinear stability analysis is very

difficult to complete, a local linear analysis is performed while the potential is calculated with nonlinear boundary conditions. The numerical stability analysis, therefore, reflects the nonlinear boundary condition effects in a global sense even though the analysis is locally linear. For moderate wave slopes, the results are consistent with those shown in Table 3−5. The numerical stability analysis, therefore, reflects the nonlinear boundary condition effects in a global sense even though the analysis is locally linear.

Figures 14 and 15 show nonlinear simulations with the same conditions as that given in Table 4. The simulation configuration is as follows : initial depth of body=1.0, body oscillation amplitude=0.5, wave number k=0.1309, number of panels on the body=10, and number of panels on the free surface=90. The stability range for the nonlinear simulations was determined to be essentially the same as for linear range indicating that a linear stability analysis is a good estimate of the nonlinear stability characteristics.

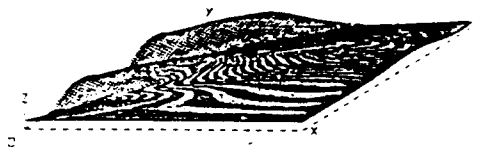

Fig. 14. Time simulation of the nonlinear potential value distribution, stable case. Two-dimensional wedge-shaped body with 45 degrees deadrise angle. 10 panels on the body and 90 panels on the free surface. Amplitude=0.5, k=0.1309, FSS number=1.0, c=0.02, without the truncation effect. Explicit fourth-order Runge-Kutta method.

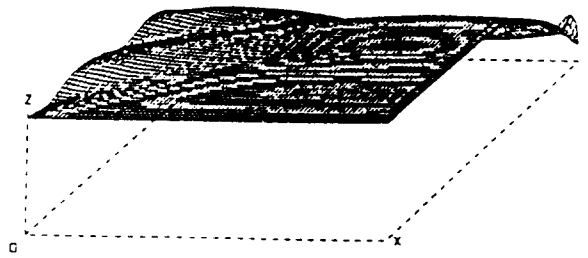

Fig. 15. Time simulation of the nonlinear potential value distribution, unstable case. Two-dimensional wedge-shaped body with 45 degrees deadrise angle. 10 panels on the body and 90 panels on the free surface. Amplitude=0.5, k=0.1309, FSS number=1.0, c=0.02, with the truncation effect. Explicit fourth-order Runge-Kutta method.

SUMMARY AND CONCLUSIONS

The goal of this paper is to better understand the complex behavior of body-free surface interaction problems, specifically the hydrodynamics associated with intersecting, non-wallsided bodies experiencing large amplitude motions. Due to the nonlinearities in the free surface boundary conditions, this problem is generally only tractable through computation and simulation. Previous studies have encountered numerical instabilities restricting the usefulness of this method. Either the simulation program stops due to floating point difficulties or smoothing techniques are applied raising questions about the validity and accuracy of the computed values.

The purpose here is to examine the fundamental causes and solutions surrounding numerical stability and instability and their subsequent effects on hydrodynamic modeling. Analytic determi-

nation and evaluation of stability regions have been completed leading to closed form solutions for stability criteria. These criteria have been supported by numerical time simulations.

Initially, simple models for the hydrodynamics are developed yielding basic information on the importance of various parameters and algorithms used in the problem solution schemes. When closed form analytic solutions are not available, this approach gives confidence in numerical results by increasing the level of complexity of the model to finally include the fully nonlinear free surface boundary conditions. Based upon the results presented here, the following conclusions are made:

• By adding a constant to the Green function, the stability characteristics of a particular time stepping algorithim may be changed. This method is effective in two dimensions with open boundary problems, but generally not effective in three dimensions or for closed boundary problems.

• The radiation condition is important to stability considerations in two-dimensional numerical analysis but less so in three dimensions. In the far-field open boundary problem, the effect of the truncation limit plays a significant role in the stability analysis. However, in the three-dimensional problem, no similar effect is observed for the cases studied in this paper. Faltinsen's method(Faltinsen (1977)) for the radiation boundary is apparently unstable but may be approximately valid until the wave propagated from the body reaches the outer boundary.

• The conditional/unconditional stability or instability of various time-stepping schemes has been demonstrated. As shown in the above sections, an explicit Euler scheme is *unconditionally unstable* and other schemes, such as the implicit-like fourth-order Runge-Kutta schemes are *conditionally stable.*

• Moderate nonlinearities do not produce significantly different stability regions than equivalent linear problems. This suggests that a preliminary stability analysis can be completed prior to actual simulation of the fully nonlinear problem by applying the von Neumann or matrix methods to linearized boundary conditions on the mean surfaces.

• Based upon axisymmetric flow analysis, three-dimensional problems appear to have larger stability regions than similar two dimensional ones.

• Figure 12 illustrates that errors expanded in terms of the eigen vectors of the [D] matrix have components with different decay rates. Those components that lie on the unit circle neither grow nor decay, while those that are within the unit circle are damped. This suggests the possibility of designing an algorithm that selectively damps unwanted components(i. e. frequencies) while minimizing the numerical dissipation of others.

• Numerical stability does not guarantee accuracy in either computation or modeling. For example, bodies characterized by low deadrise angles or high entrance velocities will produce jet-like flows. The computer code that this work is based upon could not successfully calculate such flows. While the time-stepping algorithm is stable, during simulation the formation of a jet near the intersection point leads to numeric overflow. At the intersection point, the free surface forms a thin sheet parallel to the body. The narrow distance between the body surface and the jet surface causes difficulties in the source distribution method since the influence coefficient matrix has large off-diagonal terms. This problem, jet-like impact with and without gravity, has received a considerable amount of attention, but as yet remains unsolved. See, for example Dobrovol'skaya(1969), Hughes(1972), Greenhow and Lin(1985), Greenhow(1987), Miloh(1991), Faltinsen and Zhao(1992), or Vorus(1992).

ACKNOWLEDGEMENTS

This work has been supported by the Office of Naval Research, Applied Hydrodynamics Research Program in Nonlinear Ship Hydrodynamics, Contract No. DOD-GN0014-90-J-1818.

REFERENCES

1. Troesch, A. W. and Kang, C. G., "Evaluation of Impact Loads Associated with Flare Slamming," STAR Symposium, Pittsburgh, 1988.
2. Kang, C. G. and Troesch, A. W., "Nonlinear Interaction Between Axisymmetric Submerged Bodies and the Free Surface in Water of Infinite Depth," Seminar on Ship Hydrodynamics, Seoul National University, 1988.
3. Longuet-Higgins, M. S., and Cokelet, E. D., "The Deformation of Steep Surface Waves on Water," *Proc.* R. Soc. Rond. A350, 1976, pp. 1~26.
4. Faltinsen, O. M., "Numerical Solutions of Transient Nonlinear Free-Surface Motion Outside or Inside Moving Bodies," *2nd. Num. Hydr.*, 1977.
5. Vinje, T. and Brevig, "Breaking Waves on Finite Water Depths, A Numerical Study," *Norw. Inst. Tech & NHL*, 1981.
6. Yeung, R. W., "Numerical Methods in Free-Surface Flows," *Ann. R. Fluid Mech.* Vol. 14, 1982, pp. 395~442.
7. Dommermuth, D. G., and Yue, D. K., "Numerical Simulations of Nonlinear Axi-Symmetric Flows with a Free Surface, *JFM*, Vol. 178, 1987, pp. 195~219.
8. Hong, S. W., Schultz, W. W., and Graebel, W. P., "An alternative Complex Boundary Element for Nonlinear Free Surface Flows," University of Michigan Program in Ship Hydrodynamics, Report No. 88-02, 1988.
9. Grilli, S. T., Skourup, J., and Svendsen, I. A., "An efficient Boundary Element Method for Nonlinear Water Waves," Comp. Eng. Anal. with Boundary Elements, 1989.
10. Baker, G. R., Meiron, D. I., and Orzag, S. A., "Generalized Vortex Method for Free Surface Flow Problems," *JFM*, Vol. 123, 1982, pp. 477~501.
11. Roterts, A. J., "A Stable and Accurate Numerical Method to Calculate the Motion of a Sharp Interface Between Fluids." *J. of Applied Math.*, 1983, 31 : 13-35.
12. Dold, J. W. and Peregrine, D. H., "Steep Unsteady Water Waves : An Efficient Computational Scheme," School of Math. in U. of Bristol, 1984.
13. Casulli, V. and Cheng, R. T., "Stability Analysis of Eulerian-Lagrangian Methods for the One-Dimensional Shallow-Water Equations," *Appl. Math. Modelling*, Vol. 14, 1990, pp. 122~131.
14. Dommermuth, D. G and Yue, D. K., "Study of Nonlinear Axisymmetric Body-Wave Interactions," *Proc.* 16th. Symp. on Naval Hydrodynamics, Berkeley, 1986.
15. Dommermuth, D. G., Yue, D. K., Lin, W. M., and Rapp, R. J., "Deep Water Plunging Breakers : A Comparison Between Potential Theory and Experiments," *JFM*, Vol. 189, 1988, pp. 423~442.
16. Kang, C. G., "Bow Flare Slamming and Nonlinear Free Surface-Body Interaction in the Time Domain," Ph. D. Thesis, University of Michigan, 1988.
17. Richtmyer, R. D. and Morton. K. W., *Difference Methods for Initial Value Problems*, Interscience Publishers, Inc., 1967.
18. Anderson, Tannaehill, and Pletcher, *Computational Fluid Mechanics and Heat Transfer*, McGraw-Hill, 1984.
19. Park, J. H., *The Numerical Stability of Nonli-*

near Floating Body Calculations, Ph. D. Thesis, University of Michigan, 1992.

20. Dobrovol'skaya, Z. N., "On Some Problems of Similarity Flow of Fluid with a Free Surface," *JFM*, Vol. 36, 1969, pp. 805~829.
21. Hughes, O. F., "Solution of the Wedge Entry Problem by Numerical Conformal Mapping," *JFM*, Vol. 56, 1972, pp. 173~192.
22. Greenhow, M. and Lin, W. M., "Numerical Simulation of Nonlinear Free Surface Flows Generated by Wedge Entry and Wavemaker Motions," 4th Int. Conf. on Num. Ship Hydro, 1985.
23. Greenhow, M., "Wedge Entry into Initially Calm Water," *Applied Ocean Research*, Vol. 9, No. 4, 1987.
24. Miloh, T., "On the Oblique Water-Entry Problem of a Rigid Sphere, "*Journal of Engineering Mathematics*, 25, pp. 77~92, 1991.
25. Faltinsen, O. and Zhao, R., "Slamming on the Wetdeck of Multihulls," Seventh International Workshop on Water and Floating Bodies, Val de Reuil, France, 1992.
26. Vorus, W. S., "An Extended Slender Body Model for Planing Hull Hydrodynamics," SNAME Section Meeting, Cleveland, Ohio, 1992.